SIMULATING THE AIR-FLOW FIELDS OF DIFFERENT SPUNBONDING DRAWING CONDUITS

by

Li-Li WU and Ting CHEN*

College of Textile and Clothing Engineering, National Engineering Laboratory for Modern Silk, Soochow University, Suzhou, China

Original scientific paper
https://doi.org/10.2298/TSCI1804803W

The air-flow fields of different spunbonding drawing conduits are modeled and simulated numerically. Simulated results are compared with the measured results and show good agreements with the latter. Results show that a larger narrow length and a larger contracting length can produce a higher air velocity, which is beneficial to the polymer drawing. This research is valuable to the optimal design of the spunbonding drawing conduits.

Key words: *spunbonding, drawing conduit, air-flow field*

Introduction

Melt blowing and spunbonding are two manufacturing technologies of polymer laid non-woven processes. Our research group has been studying the air-flow field and polymer drawing in the melt blowing process over decades and had some important findings [1-5]. Based on the research on melt blowing, our research group began studying the air-flow field and polymer drawing of the spunbonding process.

Different from the polymer drawing in an open space below the die in the melt blowing process, the polymer melt is drawn in a conduit in the spunbonding process. Therefore, the air-flow field of the spunbonding process is in an enclosure space while that of the melt blowing is in an open space. In the spunbonding process, the molten polymers are drawn into filaments by high velocity air in the drawing conduit. In our previous paper [6], the air-flow field of the drawing conduit was simulated and the results coincide with the measured data. In this paper, air-flow fields of different spunbonding drawing conduits are simulated and measured to investigate the effects of conduit parameters.

Air-flow field model

Figure 1 gives the shape and parameters of the drawing conduit. From the left view, it can be seen that the drawing conduit is made up of four parts. The leftmost part is a straight pipe. The air-flows into the drawing conduit through the head end of the straight pipe. The straight pipe can stabilize the turbulent air gradually, reduce the vortexes and enhance the consistency of the air-flow direction and the uniformity of the air velocity. A contracting pipe is right to the straight pipe, which connects the left straight pipe with the right narrow pipe and converts the big square cross-section of the straight pipe into the small cross-section of

* Corresponding author, e-mail: tingchen@suda.edu.cn

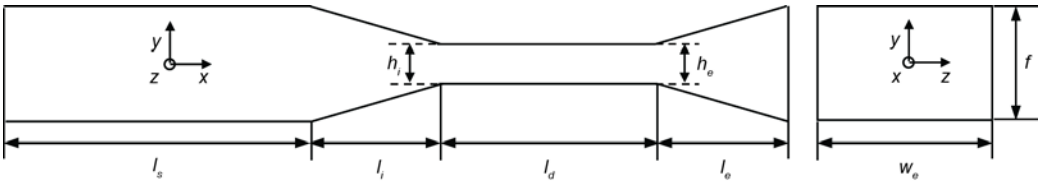

Figure 1. Sketch of the drawing conduit

the narrow pipe. The narrow pipe is right to the contracting pipe, which is the main area for the polymer drawing. An expanding pipe is right to the narrow pipe. The air-flows out of the drawing conduit from the end of the expanding pipe. Main parameters of the drawing conduits are shown in tab. 1.

Table 1. Parameters of the drawing conduits

No.	Straight length l_s [mm]	Contracting length l_i [mm]	Narrow length l_d [mm]	Expanding length l_e [mm]	Conduit height f [mm]	Entry height h_i [mm]	Exit height h_e [mm]
1	500	0	265	110	50	50	23.3
2	500	100	185	90	50	23.3	23.3
3	400	235	150	90	50	33.3	33.3
4	400	100	275	100	50	33.3	23.3
5	400	150	235	90	50	28.3	23.3

The air-flow field model is established for the drawing conduit shown in fig. 1. The k-ε model is most widely used in engineering flow simulations, which is also employed in this research as the turbulence model. The air-flow field model consists of six equations, that is, the continuity equation, momentum equation in the x-direction, momentum equation in the y-direction, energy equation, turbulent kinetic energy equation, and turbulent dissipation rate equation.

Continuity equation:

$$\frac{\partial(\rho_{\mathrm{a}} u_{\mathrm{a}x})}{\partial x} + \frac{\partial(\rho_{\mathrm{a}} u_{\mathrm{a}y})}{\partial y} = 0 \tag{1}$$

where ρ_{a} is the air density, $u_{\mathrm{a}x}$ – the x-component of the air velocity, and $u_{\mathrm{a}y}$ – the y-component of the air velocity.

Momentum equation in the x-direction:

$$u_{\mathrm{a}x}\frac{\partial u_{\mathrm{a}x}}{\partial x} + u_{\mathrm{a}y}\frac{\partial u_{\mathrm{a}x}}{\partial y} = F_x - \frac{1}{\rho_{\mathrm{a}}}\frac{\partial p_{\mathrm{a}}}{\partial x} + \frac{\theta_{\mathrm{a}} - \theta_{\mathrm{a}m}}{\theta_{\mathrm{a}m}}\mathrm{g} \tag{2}$$

where F_x is the unit mass force in the the x-direction, p_{a} – the air pressure, θ_{a} – the air temperature, $\theta_{\mathrm{a}m}$ – the ambient temperature, and g – the acceleration of gravity.

Momentum equation in the *y*-direction:

$$u_{ax}\frac{\partial u_{ay}}{\partial x}+u_{ay}\frac{\partial u_{ay}}{\partial y}=F_y-\frac{1}{\rho_a}\frac{\partial p_a}{\partial y} \tag{3}$$

where F_y is the unit mass force in the *y*-direction.

Energy equation:

$$u_{ax}\frac{\partial(\rho_a\theta_a)}{\partial x}+u_{ay}\frac{\partial(\rho_a\theta_a)}{\partial y}=\frac{\partial}{\partial x}\left[\frac{\upsilon_a+\upsilon_t}{\sigma_t}\frac{\partial(\rho_a\theta_a)}{\partial x}\right]+\frac{\partial}{\partial y}\left[\frac{\upsilon_a+\upsilon_t}{\sigma_t}\frac{\partial(\rho_a\theta_a)}{\partial y}\right] \tag{4}$$

where υ_a is the air kinetic viscosity, υ_t – the turbulent viscosity, and σ_t – the turbulence Prandtl number.

Turbulent kinetic energy equation:

$$u_a\frac{\partial(\rho_a k_a)}{\partial x}+v_a\frac{\partial(\rho_a k_a)}{\partial y}=\frac{\partial}{\partial x}\left[\frac{\upsilon_a+\upsilon_t}{\sigma_k}\frac{\partial(\rho_a k_a)}{\partial x}\right]+\frac{\partial}{\partial y}\left[\frac{\upsilon_a+\upsilon_t}{\sigma_k}\frac{\partial(\rho_a k_a)}{\partial y}\right]+$$
$$+\frac{1}{\theta_{am}}\rho_a g\frac{\upsilon_t}{\sigma_t}\frac{\partial\theta_a}{\partial x}+(P_k-\varepsilon_a)\rho_a \tag{5}$$

where k_a is the turbulent kinetic energy of air, υ_a – the air kinetic viscosity, υ_t – the turbulent viscosity, σ_k – the Prandtl number of the turbulent kinetic energy, ε_a – the dissipation rate of turbulent kinetic energy of air, and:

$$P_k=(\upsilon+\upsilon_t)\left[2\left(\frac{\partial u_{ax}}{\partial x}\right)^2+2\left(\frac{\partial u_{ay}}{\partial y}\right)^2+\left(\frac{\partial u_{ax}}{\partial y}+\frac{\partial u_{ay}}{\partial x}\right)^2\right]$$

Turbulent dissipation rate equation:

$$u_{ax}\frac{\partial(\rho_a\varepsilon_a)}{\partial x}+u_{ay}\frac{\partial(\rho_a\varepsilon_a)}{\partial y}=\frac{\partial}{\partial x}\left[\frac{\upsilon_a+\upsilon_t}{\sigma_\varepsilon}\frac{\partial(\rho_a\varepsilon_a)}{\partial x}\right]+\frac{\partial}{\partial y}\left[\frac{\upsilon_a+\upsilon_t}{\sigma_\varepsilon}\frac{\partial(\rho_a\varepsilon_a)}{\partial y}\right]+$$
$$+\rho_a(C_{\varepsilon1}P_k-C_{\varepsilon2}\varepsilon_a)\frac{\varepsilon_a}{k_a}-\frac{1}{\theta_{am}}gC_{\varepsilon1}\frac{\varepsilon_a}{k_a}\frac{\upsilon_t}{\sigma_t}\frac{\partial(\rho_a\theta_a)}{\partial x} \tag{6}$$

where σ_ε is the Prandtl number of the turbulent dissipation rate, $C_{\varepsilon1}$ and $C_{\varepsilon2}$ are constants in the standard k-ε model.

Because of the high Renault numbers of air-flow in the drawing conduit, coefficients of turbulence model are:

$$C_\mu = 0.09,\quad C_{\varepsilon1} = 1.44,\quad C_{\varepsilon2} = 1.92,$$
$$\sigma_k = 1.0,\quad \sigma_\varepsilon = 1.3,\quad \sigma_t = 0.85$$

Boundary conditions

There are three types of boundary conditions, *i. e.* the inlet, outlet and wall. Figure 2 shows the air-flow field boundaries. The upstream section is the entrance of the drawing conduit (left). The downstream section is the exit of the drawing conduit (right). The internal face of the drawing conduit subjects to the boundary condition of wall.

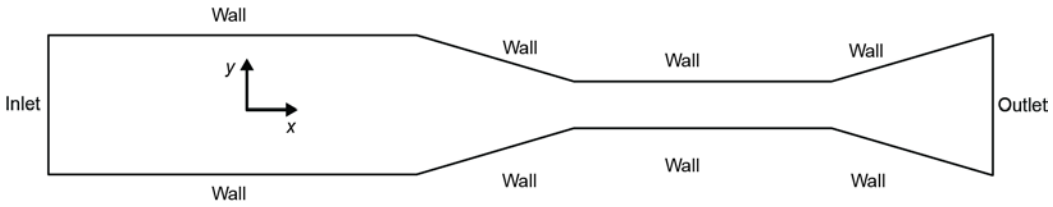

Figure 2. Boundary conditions of the air-flow field

(1) The conditions of upstream sections (inlet):

$$u_{ax} = u_{ax0}, \quad u_{ay} = u_{ay0}, \quad \theta_a = \theta_{a0}, \quad k_a = 0.06(u_{ax0}^2 + u_{ay0}^2), \quad \varepsilon_a = 0.06\frac{u_{ax0}^3 + u_{ay0}^3}{f}$$

(2) The conditions of downstream section (outlet):

$$\frac{\partial u_{ax}}{\partial x} = \frac{\partial \theta_a}{\partial x} = \frac{\partial k_a}{\partial x} = \frac{\partial \varepsilon_a}{\partial x} = 0, \qquad u_{ay} = 0$$

(3) The conditions of the internal face of the drawing conduit (wall):

$$u_{ax} = 0, \qquad u_{ay} = 0, \qquad \frac{\partial \theta_a}{\partial x} = 0, \qquad k_a = 0, \qquad \varepsilon_a = 0$$

Results and discussion

The computational fluid dynamics software FLUENT is utilized to simulate the air-flow fields of the drawing conduits. The initial air velocity and temperature are 15 m/s and 20 °C, respectively. Conduit parameters are shown in tab. 1. Figures 3-7 are the air velocity vector diagrams. The air keeps steady flow status when entering the drawing conduit from the head end of the straight pipe. When approaching the narrow pipe, with the narrowing of the air-flow area, the air velocity gradually increases and a strong air jet forms. The maximum air velocity is achieved within the narrow pipe. Behind the narrow pipe, there is the expanding pipe where the air-flow area becomes larger and larger. Thus in the expending pipe, the air velocity reduces with the enlargement of the conduit sectional area. All through the narrow pipe, the air keeps very large velocities along the spinneret axis, which is favorable to the polymer drawing. In the expanding pipe, with the decrease of the air velocity, the polymer threadline velocity also decreases gradually and the threadlines relax and flutter, which is advantageous to the random laying of nonwoven fibers.

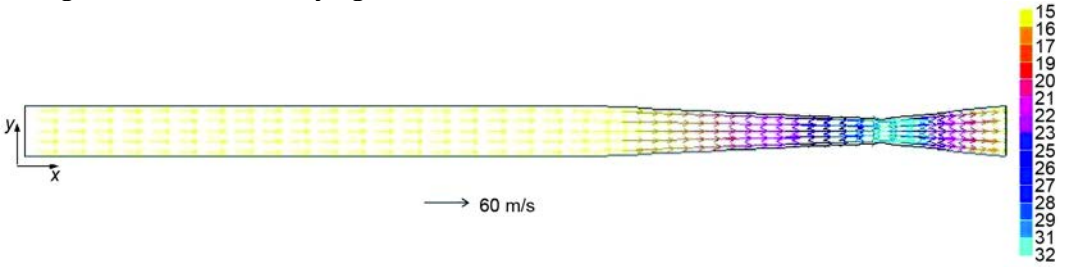

Figure 3. Air velocity vector of conduit 1 (*for color image see journal web site*)

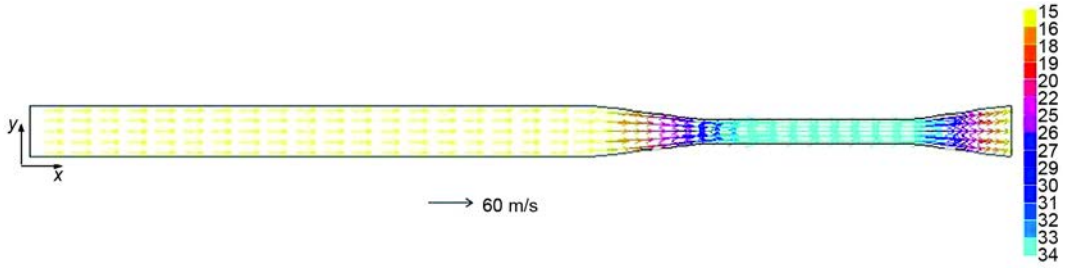

Figure 4. Air velocity vector of conduit 2 (*for color image see journal web site*)

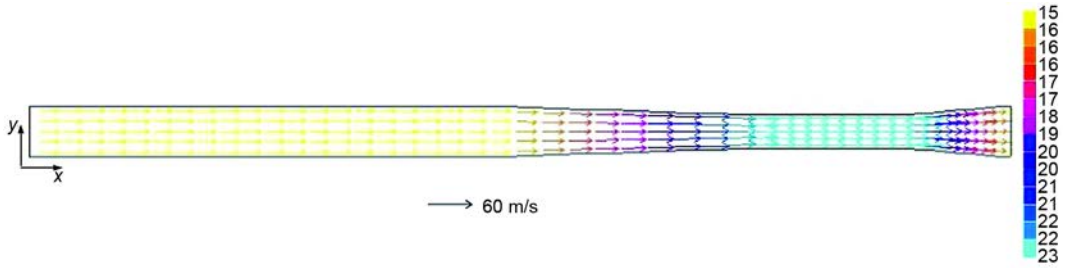

Figure 5. Air velocity vector of conduit 3 (*for color image see journal web site*)

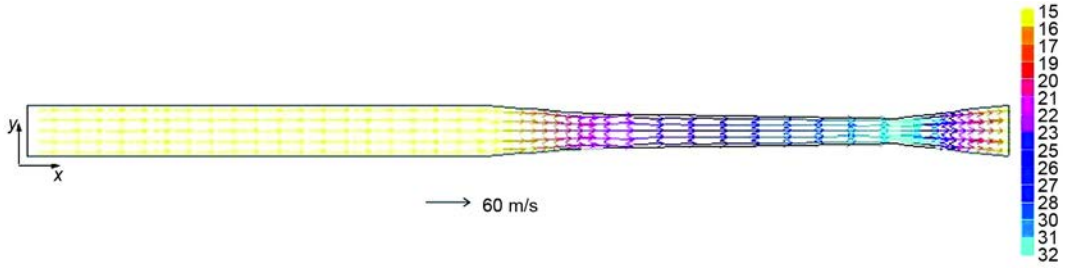

Figure 6. Air velocity vector of conduit 4 (*for color image see journal web site*)

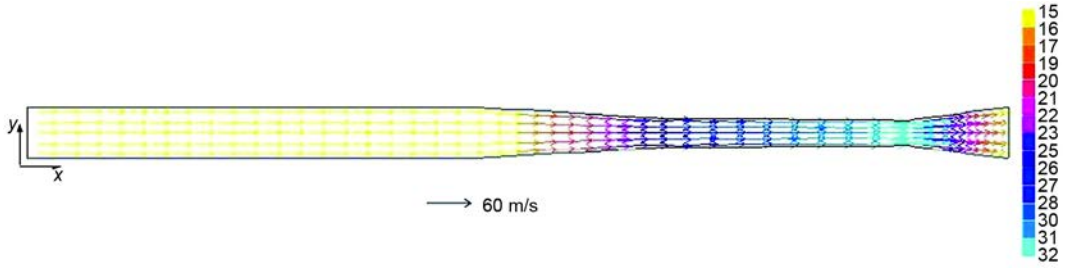

Figure 7. Air velocity vector of conduit 5 (*for color image see journal web site*)

It can be found from figs. 3-7 that air velocities in conduit 3 are the highest. Although the sum of the contracting, narrow and expanding length of conduit 3 is large, its maximum velocity is the lowest because of its smallest narrow length. It can be seen that larger contracting length can increase the air velocity. For example, the sum of the narrow and ex-

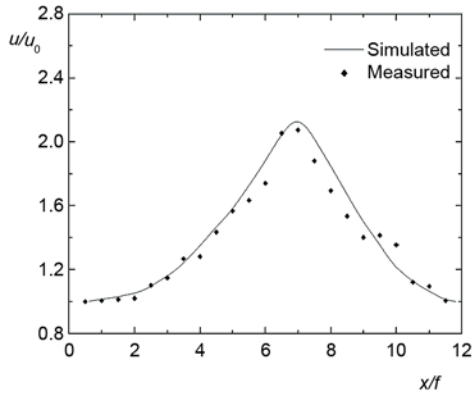

Figure 8. Simulated and measured velocity in conduit 1

panding length of conduit 1 and conduit 4 is 375 mm. However, their contracting lengths are 0 and 100 mm, respectively. Since conduit 1 is short of the transition from the straight section to the narrow section, the air speeds up inadequately, the left part of the narrow section is condemned to speed up the air which is the responsibility of the contracting section. The airflows out of the narrow section with a lower velocity. Therefore, air velocities in conduit 1 are lower than those in conduit 4.

In order to verify the air-flow field model, a particle image velocimeter is employed to measure the air velocity in the drawing conduit [7]. Figures 8-12 give the simulated and measured air velocities. It can be seen from these

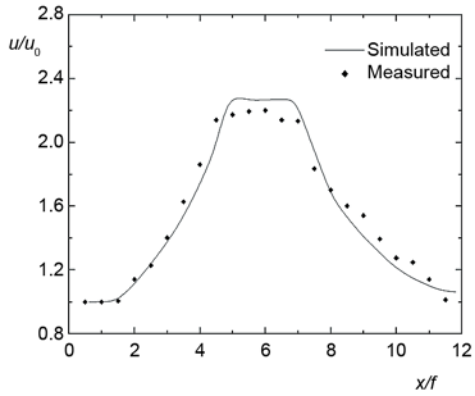

Figure 9. Simulated and measured velocity in conduit 2

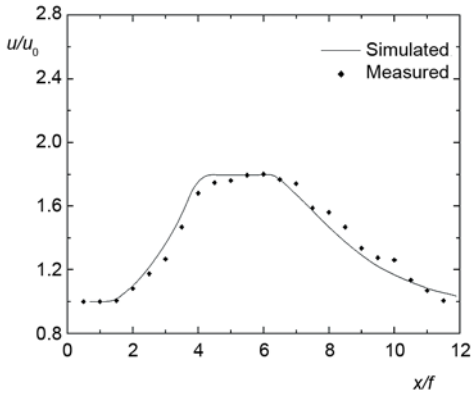

Figure 10. Simulated and measured velocity in conduit 3

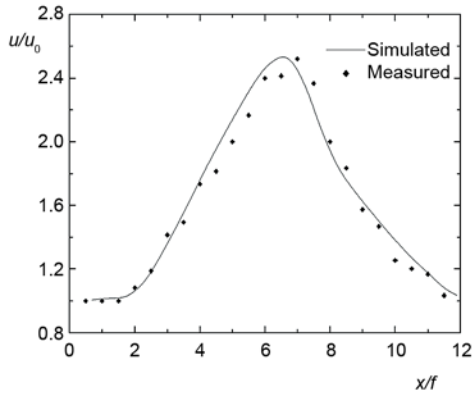

Figure 11. Simulated and measured velocity in conduit 4

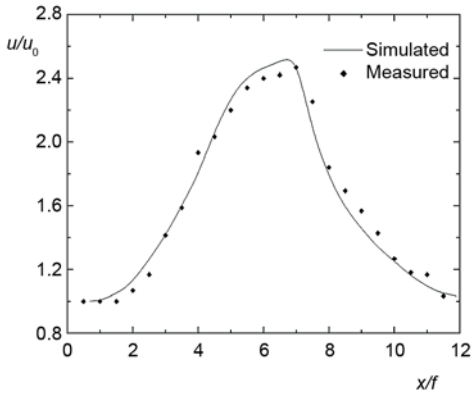

Figure 12. Simulated and measured velocity in conduit 5

figures that the simulated velocities tally well with the measured velocities, which indicates that the numerical simulations of the air-flow field of the spunbonding drawing conduits are correct and effective. Figures 11 and 12 show that air velocities in conduit 4 and conduit 5 are higher than those at the same horizontal position in other three conduits and the maximum velocity can achieve 2.5 times of the initial air velocity, which is beneficial to drawing the polymer melt. Because the contracting length of conduit 5 is larger than that of conduit 4 and the narrow and expanding length of conduit 4 is larger than those of conduit 5, the maximum air velocity of conduit 5 emerges a little earlier than conduit 4. The maximum air velocity in conduit 3 is the lowest and is only 1.8 times of the initial air velocity. Therefore, both larger narrow length and larger contracting length of drawing conduits can produce higher air velocities.

Conclusion

The air-flow fields of different spunbonding drawing conduits are modeled and simulated numerically. Simulated results are compared with the measured results and show good agreements with the latter. Results show that both a larger narrow length and a larger contracting length of drawing conduits can produce a higher air velocity, which is beneficial to the polymer drawing. This research is valuable to the optimal design of the drawing conduits in the spunbonding process.

Acknowledgment

The work is supported financially by the National Natural Science Foundation of China under Grant No. 51303121, Nantong Applied Basic Research Project under Grant No. GY12016027 and Priority Academic Program Development of Jiangsu Higher Education Institute.

References

[1] Chen, T., Huang, X., Air Drawing of Polymers in the Melt Blowing Nonwoven Process: Mathematical Modelling, *Modelling and Simulation in Materials Science and Engineering*, *12* (2004), 3, pp. 381-388
[2] Chen, T., *et al.*, Modeling the Air-Jet Flow Field of a Dual Slot Die in the Melt Blowing Nonwoven Process, *Textile Research Journal*, *74* (2004), 11, pp. 1018-1024
[3] Chen, T., *et al.*, Numerical Computation of the Fiber Diameter of Melt Blown Nonwovens Produced by the Inset Die, *Journal of Applied Polymer Science*, *111* (2009), 4, pp. 1775-1779
[4] Cheng, Y., *et al.*, Numerical Simulation of the Air Flow Field in the Melt Blowing Process with an Auxiliary Nozzle, *Heat Transfer Research*, *44* (2013), 5, pp. 473-382
[5] Wu, L. L., *et al.*, Verifying the Polymer Drawing Model of Melt Blowing using Factory Production Data, *Thermal Science*, *19* (2015), 4, pp. 1466-1467
[6] Wu, L. L., *et al.*, Study on the Air Flow Field of the Drawing Conduit in the Spunbonding Process, *Thermal Science*, *19* (2015), 4, pp. 1443-1444
[7] Zhao, B., Study on the Air Drawing in Spunbonding Nonwoven Process, Ph. D. thesis, Donghua University, Shanghai, China, 2009

Paper submitted: December 17, 2017
Paper revised: February 10, 2018
Paper accepted: February 15, 2018